Biodegradable Microparticles for Simultaneous Detection of Counterfeit and Deteriorated Edible Products

Ivan Rehor, Sophie van Vreeswijk, Tina Vermonden, Wim E. Hennink, Willem K. Kegel, and Huseyin Burak Eral*

In an era of globalized trade relations where food and pharmaceutical products cross borders effortlessly, consumers face counterfeit and deteriorated products at elevated rates. This paper presents multifunctional, biodegradable hydrogel microparticles that can provide information on the authenticity and the potential deterioration of the tagged food or pharmaceutical formulations. These microparticles integrate spatially patterned authenticity code with two sensors—the first one detects possible presence of pathogenic microbes through monitoring pH while the second one identifies products stored above optimal temperatures via optical monitoring of the microparticle degradation. Particles are synthesized from a biocompatible polymer and a photoinitiator, dextran modified with 2-hydroxyethylmethacrylate and riboflavin, respectively, using a continuous, high throughput method stop-flow lithography. The proposed synthesis approach also enables crosslinking with visible light bringing about additional flexibility to flow lithography. Model liquid and solid food and pharmaceutical products are successfully labeled with microparticles and the functionality of the sensors in aqueous solutions is demonstrated.

Dr. I. Rehor, S. van Vreeswijk, Prof. W. K. Kegel,
Prof. H. B. Eral
Van't Hoff Laboratory for Physical and Colloid
Chemistry, Debye Institute for Nanomaterials Science
Utrecht University
3584 CH, Utrecht, The Netherlands
E-mail: h.b.eral@tudelft.nl

Prof. T. Vermonden, Prof. W. E. Hennink
Department of Pharmaceutics, Utrecht Institute for
Pharmaceutical Sciences
Utrecht University
3584 CH, Utrecht, The Netherlands

Prof. H. B. Eral
Process & Energy Laboratory
3ME Faculty
TU Delft
2628 CB, Delft, The Netherlands

The ORCID identification number(s) for the author(s) of this article can be found under https://doi.org/10.1002/smll.201701804.

1. Introduction

Food and pharmaceutical products traded across the globe must fulfill strict quality criteria. However, potentially harmful products still appear on the market, raising serious public health concerns. Such products are either manufactured in substandard quality—a typical feature of counterfeit products[1–4]—or undesired properties develop during inappropriate storage.

Counterfeit consumer goods are on the rise globally. The situation is extraordinarily alarming in the case of pharmaceutical products, ≈10% of all pharmaceuticals sold worldwide are counterfeits or of substandard quality, reaching 30% in developing countries.[1,2,5,6] Equally alarming evidence can be found in food industry—in 2008 three hundred thousand babies were victimized along with six reported deaths due to substandard baby milk powder in China.[7–9] Use of authenticity labels on pharmaceuticals, such as special prints, holograms, or other features, are a key part of

the anticounterfeiting strategy recommended by World Health Organization (WHO).[10] Authenticity labels using isotopes,[11] chemicals,[12,13] nanoparticles,[14] or microparticles[15] were described in the literature and several solutions are already commercialized (DNATrax,[16] Truetag,[17] Taneeh[18]). However, the detection of these systems requires special instrumentation (dedicated spectrometer[17,18] or polymerase chain reaction kit[16]), making verification by the end customer difficult.

Microscale lithographic objects emerged as a logical alternative to nanoscale and molecular taggants as their size allows for nondestructive authentication using optical microscopic devices, which are easily accessible to the end customers thanks to rapid development of low-cost portable microscopic technologies.[19] Recent developments in micromanufacturing techniques allow for construction of highly elaborate micro objects that have the ability to carry the information about product, i.e., serve as a microsized barcodes. Numerous microbarcode designs are reported in literature and have been proposed for labeling pharmaceuticals,[17–22] consumer goods,[23,24] or for multiplex assays.[25] The authenticity information is conventionally stored in the particle in the form of a code (binary,[26] color,[27–30] barcode,[20,21] QR code[22]). The code is either imprinted in the barcode shape,[22,24,26] its topography[24] or, alternatively, the particle is divided into compartments of different compositions.[27,29]

Generally, direct placement of the authenticity label onto the formulation provides superior security level over a label placed on the package, as it protects from gaining false authenticity through simple repackaging.[31] If an authenticity label is to be placed directly on or into the product, it must be constructed from biocompatible material to cause no harm to the consumer. Thus, it is preferred to design barcodes based on materials that are biodegradable and that have shown good biocompatibility characteristics in biomedical and pharmaceutical applications. The previously mentioned microbarcode designs, however, consist of nondegradable substances (either inorganic or polymeric) or even contain toxic substances, such as quantum dots[27] or lanthanide salts.[29,32,33] To our best knowledge, the only biodegradable barcodes reported in literature are microfibers from polylactic-co-glycolic acid[20] or alginate.[34] In both cases, one may speculate whether proposed fiber designs provide sufficient coding capacity needed for industrial scale manufacturing (10^{10} combinations is the current standard for batch identification in pharmaceutical).

Ensuring the degustation safety directly prior consumption is as important as verifying its authenticity. Pathogen contamination and growth inside a product is a major concern, especially with foods. In USA only, 48 million people get sick, 128 000 are hospitalized, and 3000 die from foodborne diseases every year.[35] The number of casualties worldwide reaches an alarming 420 000 every year.[36] Even when not contaminated with pathogens, old or improperly stored product undergoes (partial) decomposition, which can alter its properties and, in certain cases, toxic effects arise. A notorious example from the pharmaceutical industry is the development of severe symptoms (nausea, vomiting, proteinuria, acidosis, glycosuria, and aminoaciduria) in patients treated with old, partly deteriorated tetracycline antibiotics.[37] To protect a customer from consummation/use of contaminated or deteriorated products, every product bears an expiry date. This date, however, is relevant only when a product is stored under recommended conditions. As these conditions might have been violated in the supply chain, the consumer may avoid ingesting contaminated or deteriorated products, and prevent any associated risks, only by confirming the products' integrity directly prior to consumption. Although numerous technological solutions were proposed to check, for example, pathogen presence[38] or product package integrity,[39,40] integrated commercial solutions are still missing on the market.

In this study, we report multifunctional hydrogel microparticles bearing a spatially patterned binary authenticity code capable of tagging 4.3×10^9 distinct products and two integrated sensors reporting the product safety. The ratiometric fluorescent pH sensor detects pH changes in tagged liquid products attributed to bacterial contamination—a common procedure in microbiology. The storage temperature sensor identifies products stored outside recommended storage temperature. This sensor can even detect short time (approximately several hours) exposure of the tagged product to elevated temperature and reports this information by permanent change of the particle shape. Owing to the biocompatible and biodegradable substrates used in the microfluidic synthesis, the microparticles can be placed directly on/into the edible products, providing orthogonal and more difficult to bypass security over current technologies placed on the package. We demonstrated that the developed microparticles are suitable for labeling solid and liquid formulations of model food and pharmaceutical products. The microparticles were visualized using a standard fluorescent microscope and a smartphone equipped with a low-cost lens attachment. The detection of microparticles with a common portable microscope enables rapid authenticity and product safety verification directly prior to consumption by consumers. We believe that the developed proof-of-concept multifunctional microparticles may bring about a new integrated solution in addressing the global challenge of protecting customers from consuming counterfeit and deteriorated products.

2. Results and Discussion

2.1. Particle Synthesis and Use as Authenticity Labels

Stop-flow lithography was employed as a continuous technique for microparticle synthesis possessing significantly higher production rates compared to other lithographic methods.[41] The synthesis is described in detail in the Experimental Section and schematically depicted in **Figure 1**. In the previous works dealing with stop-flow lithography (SFL), nonbiodegradable polymers (mainly polyethyleneglycol-diacrylate – PEGDA) were used as substrates for lithographic hydrogel particle synthesis.[29,42] An exception is the work of Hwang et al.,[43] in which hydrogel microparticles of simple geometries were synthesized from PEG bound to acrylates through hydrolyzable oligolactide linkers. Despite
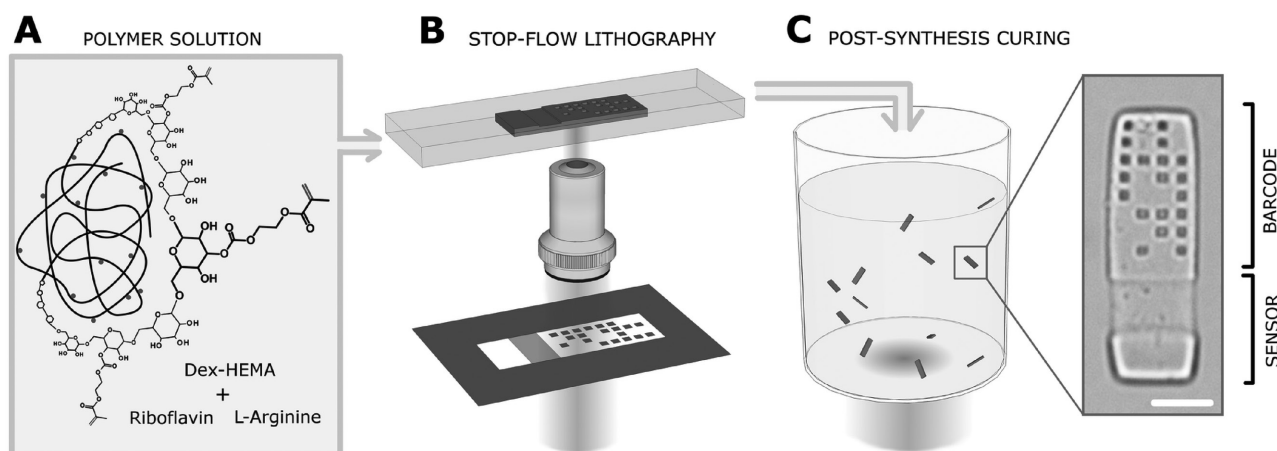
Figure 1. Scheme of the particle synthesis. A) Solution of biocompatible polymer (Dex-HEMA) and photoinitiator (riboflavin + L-arginine) in water is pumped through a microfluidic channel and B) hydrogel microparticles are synthesized by light pulses through a mask placed at the field stop of the microscope. After particles are collected and diluted, they are irradiated again to increase their crosslinking density in a postsynthesis curing step. C) The particle contains region with a binary code and sensor region used as a storage temperature sensor. Scale bar corresponds to 20 µm.

this change in chemical composition, the dominant mass fraction of the prepared hydrogels (75%) was formed by the synthetic PEG polymer. It is general practice to use natural or naturally identical compounds in food and pharmaceutical products as much as possible to avoid possible undesired side effects of synthetic compounds. For this purpose, we utilized biocompatible dextran modified with 2-hydroxyethylmethacrylate (Dex-HEMA) polymer as a substrate for hydrogels.[44] Dex-HEMA consists of a natural polymer–dextran (75% of total polymer mass) modified with 2-hydroxyethylmethacrylate moieties along the chain (scheme in Figure 1 left). The connection between HEMA and dextran is achieved through hydrolytically labile carbonate esters, and therefore, hydrogels prepared by crosslinking Dex-HEMA degrade under biological conditions.[45] Dex-HEMA hydrogel particles were previously evaluated during clinical trials in human patients as a drug delivery carrier, exhibiting no harmful side effects.[46] Also products of Dex-HEMA hydrogels possess good biocompatibility[47]—dextran is used as a plasma expander, and poly(2-hydroxyethyl methacrylate) is a polymer used in many biomedical products and other pharmaceutical applications.[44] We have used riboflavin, vitamin B2, as a fully biocompatible photoinitiator[48–50] for crosslinking Dex-HEMA. Riboflavin requires an electron donor to work as a photoinitiator. L-arginine is a natural amino acid, which has been successfully implemented as an electron donor for riboflavin.[50] Using riboflavin and arginine allowed us to avoid traditional, possibly harmful,[50,51] phenone photoinitiators, which have been used up to now with SFL. Furthermore, riboflavin is photosensitive in the visible part of the spectrum,[52] hence we could use visible light (400–490 nm) for crosslinking. Avoiding UV exposure of the hydrogel is important for future applications of our system, such as production of cell laden hydrogels or hydrogels with biologically active, UV-sensitive molecules.

In order to produce mechanically robust particles with sufficiently long shelf life, we increased the particle crosslinking density by incorporating an additional postsynthesis curing step into the synthesis procedure (Figure 1C).

After particles were flushed from the microfluidic channel, they were dispersed in a solution of riboflavin and arginine, and the whole suspension was irradiated again. In the postsynthesis irradiation, we nominally used a 365 nm UV lamp. To investigate if UV exposure can be avoided throughout the entire synthetic process, we also used a 405 nm diode laser instead of a UV lamp in several experiments (see the Experimental Section for more details). The choice of the light source in postsynthesis curing did not seem to have effect on the final stiffness or the decomposition behavior of microparticles: the particles were stiff and no degradation was visible on aqueous solutions. However, more quantitative characterization is required in order to draw a final conclusion. The microscopy images of postsynthetically cured particles are shown in Figures 1,2A, and 4. The microscopy image of microparticles synthesized without the postsynthesis curing step is provided in Figure S1 (Supporting Information).

The dimensions of synthesized particles were 100 µm × 30 µm × 25 µm (standard deviation > 7%), the first two dimensions are defined by the photomask, the third by the microfluidic channel height. The particles are large enough to be conveniently visualized using a standard laboratory microscope and, simultaneously, small enough to be completely invisible with a naked eye. The bright-field and fluorescence images (using incorporated rhodamine dye) of particles dispersed in solution are in **Figure 2**A. The particle contains binary code with 2^{32} ($\approx 4.3 \times 10^9$) combinations. Similar coding system has been commercialized with SFL-produced microgels for biomolecule analysis.[26] To demonstrate the "on-the-spot" readability of microparticles prior to consumption by the end customers, we synthesized 2× larger particles (200 µm × 60 µm × 25 µm) than our nominal size and visualized them using a cellphone camera with a microscopic lens attached (price ≈5 EUR), as seen in Figure 2B. Thanks to the larger particle size, the code is readable despite the low resolution of the low-cost portable microscope.

The particles can be dried without losing their shape. Therefore, they could be used as labels for oral solid dose (OSD) formulations, i.e., tablets and capsules, which are
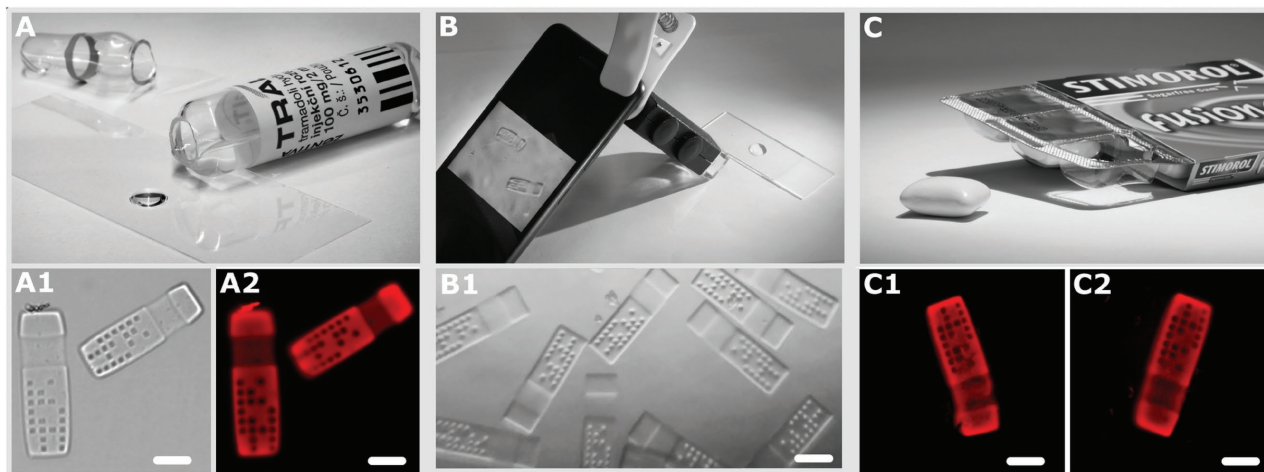
Figure 2. Model food and pharmaceutical products tagged with postsynthesis UV treated microparticles. A) Labeled intravenous solution of Tramadol painkiller, transmission (A1) and fluorescence (A2) images of microparticles dispersed inside the solution. B) Particles in solution are visualized using a low-cost microscope attached to a smartphone (B1). C) Labeled chewing gum and fluorescence microphotographs of particles on its surface (C1, C2). Scale bars correspond to 50 µm in (B1), and to 20 µm in all other images.

by far the most common formulations of pharmaceuticals. Microparticles placed on OSD formulations only have anti-counterfeiting feature, as the sensors are only usable in liquid formulations. Fluorescence dye (acrylated rhodamine B (Rh)) was covalently incorporated into the hydrogel to facilitate its reading with a fluorescent microscope.[43] The images (Figure 2C) show that the particles keep their shape after drying, and the code remains readable on a model OSD surface (chewing gum).

2.2. Sensing Functions of Particles in Aqueous Solutions

Aqueous food and pharmaceutical products (drinks, pharmaceutical oral or intravenous solutions, etc.) are in general more prone to a microbial contamination because microbes readily proliferate in aqueous solutions. The products dissolved in water also degrade faster than the dry forms of products. If the product is stored outside recommended conditions, such as elevated temperature, it can even deteriorate before the expiration date provided by the manufacturer. Therefore, we have incorporated two sensors into the microparticles that report on an actual condition of the labeled product. First, we focused on detection of a possible microbial contamination of a product. When an aqueous solution is contaminated with microbes, the solution pH drops,[53] thus, simply measuring the pH of a solution may indicate bacterial growth. This approach is routinely used in cell biology experiments, where cell growth media are labeled with phenol red, which changes its color from purple to orange upon decreasing pH, thereby reporting bacterial contamination of cell culture. Ratiometric fluorescence pH detection is a powerful method with excellent signal-to-noise ratio which possesses reliable data even when measuring samples of complex composition due to the low probability of interference with measured sample.[54] Ratiometric pH detection has been used in various bioapplications such as measuring the pH in bacterial cultures,[53] inside tissues,[55] or living cells.[56]

To create ratiometric pH sensor, we covalently incorporated methacrylated fluorescein (Fc) and Rh dyes into the hydrogel microparticles by adding them both into the pregel mixture of polymer and photoinitiator.[43] The emission intensity of the fluorescein dye is pH dependent hence it reports on a change of pH. The emission peak of Rh at different wavelength is pH independent and serves as a reference. The fluorescence dyes were chosen with respect to the commercial availability of their acrylated analogues that allow simple covalent incorporation into the hydrogel. Furthermore, fluorescein and rhodamine are easily detected by standard fluorescent microscopes, equipped with filter cubes that do not allow the freedom of choice in excitation and emission wavelength. We used low dye concentrations in the pregel mixture ($\approx 100 \times 10^{-6}$ м) to suppress fluorescence resonance energy transfer between the dyes.[57] These concentrations should be also sufficiently low to avoid any possible undesired side effects inside a body. We did an approximate estimation of the dye concentrations inside a tagged product to be below ppb (calculation can be found in the Experimental Section), which is deeply below legal toleration limits (1.5 µg of undefined impurity in daily dose).[20,58] The response of both dyes to changes in pH is plotted in **Figure 3**. The plot shows quenching of the Fc emission when the pH drops, while the Rh emission remains constant. Fc emission response to the pH change is rapid (less than 1 min) and its fluorescence intensity is fully recovered after subsequent pH increase. The ratio between Fc and Rh emissions is linearly proportional to the pH in the studied region from 6.0 to 7.5 (Figure S2, Supporting Information) and the sensitivity is less than 0.5 pH units. The presence of our sensor in a particle allows the observation of pH changes caused by pathogen growth and, thus, can prevent usage of a contaminated product by the consumers. We would like to point out, that a pH drop not always point to bacterial metabolic activity. Some pathogens do not lower the pH In fact; several changes in the product composition can alter the pH. However, many typical food contaminants (e.g., *Escherichia coli*) can be detected using simple sensor of this type.[53]
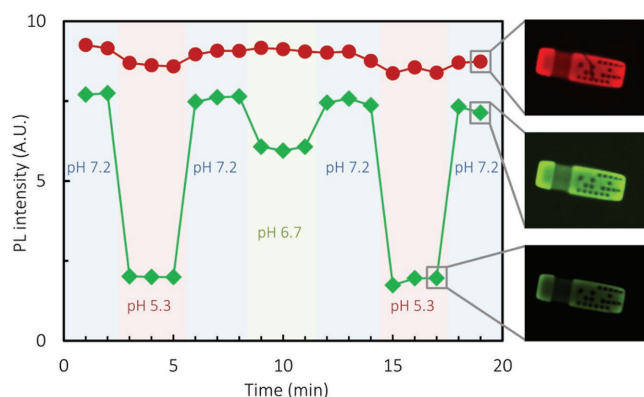
Figure 3. Plot of the particle's fluorescence response (green and red) to sudden pH changes. Emission intensities of both dyes of ratiometric sensor (fluorescein – responsive, rhodamine – reference) are followed over time, while pH is changed every 3 min by buffer exchange.

Notably, the pH check using our fluorescent sensor can be performed through a transparent package and therefore does not disturb the intactness of the product, unlike a conventional pH test.

Even when not contaminated by microbes, food and pharmaceutical products undergo aging and lose their original quality over long term storage. The storage conditions, in particular temperature is crucial in determining the deterioration rate of a product and, ultimately, the real expiration date. Therefore, we developed a storage temperature sensor to identify products stored outside the suggested temperature range. The Dex-HEMA polymer chemically degrades in aqueous solutions as the carbonate ester groups, connecting HEMA to dextran hydrolyze.[44,45] Due to the hydrolysis, polymer chains become more loosely connected to each other, which results in a swelling of a Dex-HEMA hydrogel[45] and subsequently leads to the disintegration of the entire particle. We decided to use the hydrogel swelling as a measure of its hydrolysis state. We have also developed an alternative methodology for this measurement, using the fluorescence decay of the particles during hydrolysis—more details can be found in the Supporting Information. Preliminary experiments of particle hydrolysis in water solution showed that the relative increase in overall particle dimensions (length and width) was only 20% during hydrogel hydrolysis before particles completely dissolved, which was not sufficient for precise determination of a hydrolysis state (plot in **Figure 4**A). Therefore, we designed our microparticles in the following way to increase the hydrogel response to the hydrolysis. The relative swelling of Dex-HEMA hydrogels during hydrolysis decreases with their increasing initial crosslinking density.[45] The crosslinking density of our hydrogel particle is dependent (among other parameters) on the amount of light absorbed by the pregel solution during SFL synthesis. Thus we added a new segment into the photomask—a semitransparent stripe designed to transmit only 70% of light in order to decrease the irradiation intensity and subsequently the crosslinking density in the corresponding area of the particle—the "gray" segment. Indeed in the performed ageing experiments the "gray" segment in the particle exhibited a significantly steeper swelling curve, compared to
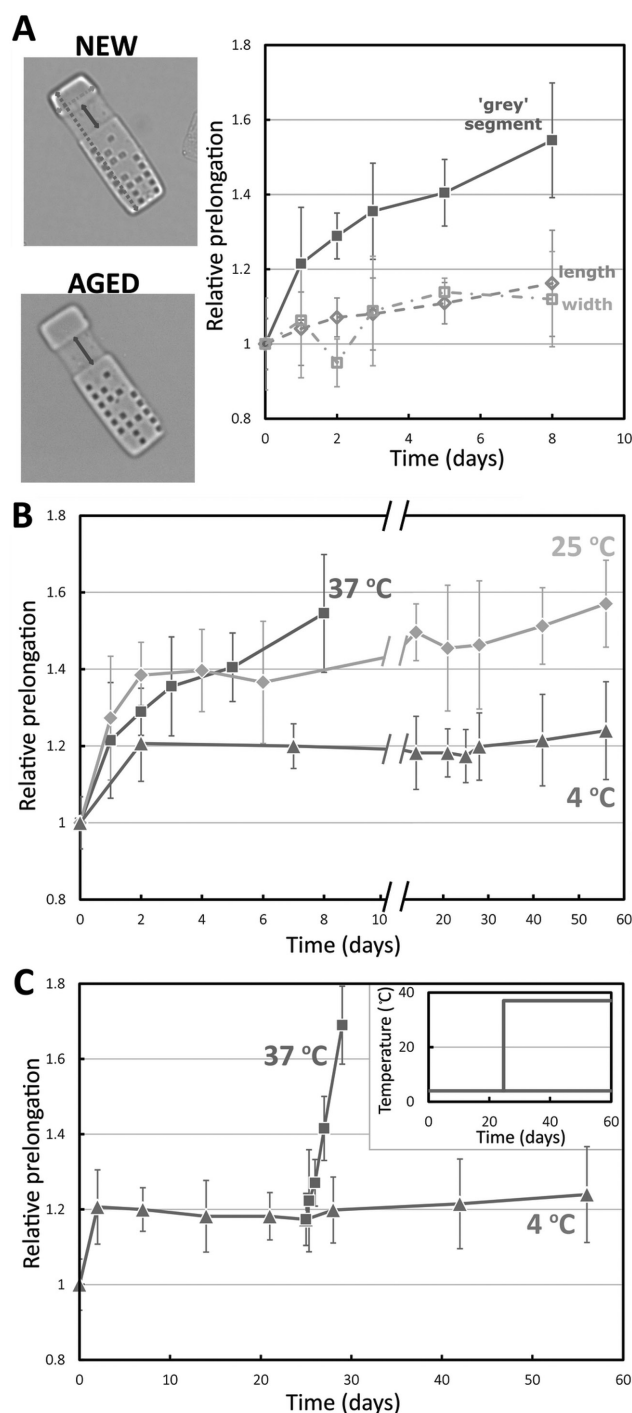

Figure 4. Tunable and temperature dependent swelling behavior of microparticles. A) Microparticles stored in solution swell over time as the crosslinks in Dex-HEMA gel degrade (upper inset – prior to aging, lower – aged 8 d at 37 °C). The plot shows relative elongation along different directions in the microparticle over time. B) Relative prolongation of the sensory segment in particles stored at different temperatures (4, 25, and 37 °C – triangles, diamonds, and squares, respectively). C) Relative swelling of "gray" segment in particles stored at 4 °C (triangles), compared to swelling in particles exposed to 37 °C after 24 d at 4 °C (squares). Temperature profile is given in inset.

the rest of the particle and reached ≈150% of its original length, before entire particle dissolved (Figure 4A). Notably, the large error bars in the plots are due to the nonuniformity

© 2017 Wiley-VCH Verlag GmbH & Co. KGaA, Weinheim

of the particles—each particle differs from each other in the crosslinking density and thus in the hydrolysis speed. We ascribe this nonuniformity to the poor control over experimental conditions during the postsynthesis curing step as omitting this step yields highly uniform particles. This issue is discussed in more detail in the Supporting Information. We are currently working on improving our experimental setup.

Figure 4B shows temperature dependency of the "gray" segment swelling—the segment elongated faster when stored at elevated temperatures. The non-monotonic rates of the swelling in time are roughly similar to previously reported data on macroscopic Dex-HEMA hydrogels.[45] Next, we focused on the response of the "gray" segment to a sudden temperature change. We kept the particles at 4 °C for approximately three weeks, then divided the sample into two and heated up one half to 37 °C. The "gray" segments of the particles exposed to the elevated temperature swelled rapidly (Figure 4C) and its elongation became significant (t-test) already after 24 h exposure. In summary, the sensor elongates faster when stored at elevated temperatures and even a short term exposure to an elevated temperature is reported by the sensor. The information is read simply by measuring the "gray" segment length using a standard light microscope. This test can distinguish the product stored at recommended temperature, from a product exposed, even for a limited time, to an elevated temperature).

3. Conclusion

We developed a flow lithography process for manufacturing microparticles integrating authenticity and sensory functions, with nonharmful biodegradable chemicals. By careful choice of implemented chemistry, we avoided the commonly used UV irradiation in the lithographic process and replaced it with visible light. Synthesis of the microparticles with visible light brings about flexibility in experimental design (choice of microscope objectives, light source) and facilitates loading the hydrogels with a UV sensitive cargo, such as living cells or UV-cleavable drugs.

To demonstrate the feasibility of our method, we synthesized multifunctional biodegradable hydrogel microparticles as taggants for food and pharmaceutical products. The microparticles provide simultaneous information on the product authenticity and safety directly prior to consumption. The authenticity information is embedded in the microparticle topography as a binary code. The product safety of liquid products—the presence of the pathogens and the potential product deterioration due to improper storage—is reported through the sensors embedded in the microparticle structure. The authenticity code and the sensor information are acquired with a standard bright-field/fluorescent microscope (or even a cellphone in the case of authenticity). Incorporation of the sensors into the microparticle itself offers all-in-one solution with potentially broader applications than the previously proposed alternatives placed on the packages.[59]

The microparticle production is scalable, due to the continuous nature of stop-flow lithography so it can be implemented in industrial scale.[26] Simultaneously, it is a difficult technology to counterfeit, requiring advanced equipment and microfluidic skills. The natural degradation of the microparticles and the ability to directly place them on the products also limits possibilities for unauthorized manipulation, repackaging, reprocessing, and dilution of original products, which is a common practice in counterfeiting. The proposed multifunctional system is orthogonal to other available methods therefore; it brings an additional layer of security, recommended in the WHO strategy to fight counterfeiting.

Our results demonstrate early model and proof-of-concept verification of the product authenticity and condition "on-the-spot" directly prior to consumption. We believe with further critical thinking and design the presented barcode system can contribute to public safety. Thus, the multifunctional microparticles represent an integrated approach combining a microfluidic/lithographic technique that sculptures the microscale shape with molecular level chemical design enabling sensory and biodegradability functionality to potentially protect consumers from potentially harmful counterfeit and deteriorated products.

4. Experimental Section

Materials: 1,1′-Carbonyldiimidazole, HEMA, 4-methoxyphenol, Na_2SO_4, riboflavin, L-arginin, fluorescein O-methacrylamide, sodium azide, and *N,N*-dimethylaminopyridin (DMAP) were purchased from Sigma-Aldrich. Methacryloxyethyl thiocarbamoyl rhodamine B was purchased from Polysciences. SYLGARD 184 silicone elastomer kit, used for production of polydimethylsiloxane (PDMS) channels, was purchased from Dow Corning. Dextran from Leuc. Spp., Mr ≈ 40 kDa (Sigma-Aldrich) was dried over phosphorous pentoxide under vacuum at room temperature (RT) overnight. Molecular sieves (3 Å, Sigma-Aldrich) were dried under vacuum at 250 °C for 5 h and used fresh. Dichloromethane, DMSO (HPLC, dried over sieves), reverse osmosis water was used in experiments (18.2 MΩ).

Synthesis of Dex-HEMA: HEMA-imidazoyl carbamate (HEMA-CI) was synthesized according to the previously published procedures.[44] The details can be found in the Supporting Information. 2-Hydroxyethyl methacrylate modified dextran was synthesized according to previously published procedures,[44] with minor modifications. Briefly: Dextran (1 g) was placed into a 40 mL flask together with *N,N*-dimethylaminopyridin (200 mg, 1.6 mmol). DMSO was added (9 mL) and the flask was purged in three sequential steps of nitrogen and vacuum. Dextran and DMAP were dissolved under stirring (temperature was raised up to 70 °C to facilitate dissolution). HEMA-CI (430 mg of 90% product, 1.9 mmol) was added dropwise to the reaction mixture at RT. The reaction was conducted at RT under the inert atmosphere for 3 d. Sodium phosphate buffer (20 mL, 0.1 M, pH = 7.4) was added and the mixture was dialyzed against water for 4 d at 4 °C (the water was exchanged every 12 h). The resulting solution was freeze-dried yielding 1.15 g of the product (86%). The obtained product was characterized using ^1H NMR. δH (400 MHz, D2O) 6.02(bs, 0.33H, =CH'H'' HEMA), 5.61(bs, 0.34H, =CH'H'' HEMA), 4.85(bs, 1H, O−CH−O Dex), 4.39(bs, 0.70H, N−CO−O−CH_2 HEMA), 4.32(bs, 0.70H, C−CO−O−CH_2 HEMA), 4.10-3.10 (m, 6H, Dex), 1.80(bs, 0.97H, −CH_3 HEMA).

The number of HEMA groups per ribose unit of dextran (degree of substitution – DS) was calculated from an ^{1}H NMR spectrum, comparing integral intensity of six dextran protons multiplet between 3.2 and 4.1 ppm (I_{DEX}) to integral intensity of methylene group of HEMA at 1.75 ppm (I_{HEMA}) as stated in Equation (1). The degree of substitution of Dex-HEMA used in the study was 0.35:

$$DS = \frac{2 \times I_{HEMA}}{I_{DEX}} \tag{1}$$

Pregel Nominal Composition: 50 mg of Dex-HEMA was dissolved in 180 µL of the riboflavin saturated solution in water. After complete dissolution, L-arginine (20 µL of 5% w/w solution) was added. Then methacryloxyethyl thiocarbamoyl rhodamine B (2 µL, 12×10^{-3} M in DMSO) was added or/and fluorescein o-methacrylate stock solution (4 µL, 62×10^{-3} M in DMSO) were added.

Microfluidic Channel Production: PDMS microfluidic channels were fabricated as previously described.[60] First, the mixture of silicone elastomer base (35 g) and the curing agent (5 g) was poured over a silicon wafer with positive relief channels patterned with SU-8 photoresist (Microchem). The thickness of the PDMS layer was around 8 mm. The wafer with PDMS was kept at 70 °C overnight then the PDMS layer was cut and peeled off. Next, a 1 mm hole was punctured through the PDMS on each end of the channel using biopsy needle. The channels were attached to glass slides with a thin layer of spin-coated and semicured (70 °C, 28 min, ratio base: curing agent = 10:1 vol/vol) PDMS layer. The whole device was then cured at 70 °C overnight. Ready channels of width 300 µm, height 30 µm, and length 2 cm were rinsed with ethanol MilliQ water and dried with a stream of nitrogen.

Microscope Setup: Inverted microscope (Nikon Ti-E) was used for microparticle production and observation. An Hg lamp (Nikon Intensilight) was used as the light source for photocrosslinking (<490 nm using dichroic mirror). The shutter of the source was controlled remotely. The photomasks were designed as a bitmap, transferred to diapositive slide, which was subsequently developed using wet photo process. A UV absorbing layer was present on the diapositive slide hence all light below 400 nm was blocked. For fluorescence microscopy cube filters for RITC and FITC (Semrock) were used.

Microparticle Synthesis: The details of the SFL setup were described previously.[42,61,62] Compressed air was used to generate a pressure difference to induce flow in the channel. The input pressure was set to 0.5 psi using a pressure gauge. The gauge outlet was connected to a three-way solenoid valve, which allows switching rapidly between the atmospheric pressure (stop) and the input pressure (flow). The solenoid valve was controlled remotely. An inverted microscope was used for particle production. The PDMS channel was placed on the microscope stage. The 0.8 mm needle with flat end was filled with the pregel solution (50 µL, standard composition—see above), inserted into the inlet hole and attached to the solenoid valve with a tube. A flat-end needle was inserted to the outlet hole and served for the collection of crosslinked particles. The solenoid valve and the Hg lamp shutter were programmed to cycle in a following way: I. PURGE: valve opened, shutter closed – 3 s; II. STOP: valve closed, shutter closed – 1 s; III. PRINT: valve closed, shutter open – 1.2 s. Then the shutter was closed and simultaneously the valve was opened and the whole cycle was repeated. To avoid sticking of the synthesized particles to the channel walls, the irradiation position was changed by 150 µm in the channel every ten irradiations using the motorized stage. When the end of the channel was reached, the exposure spot was reset to the original position. After synthesis (typically several thousands of particles were prepared in one run), the channel was purged with MilliQ water (500 µL) and particles were collected into an Eppendorf tube. For the postsynthetic curing step, 500 µL of riboflavin saturated solution and 120 µL of L-arginine solution (5% w/w) was added to the Eppendorf with collected particles. The Eppendorf was then placed under UV lamp (Blak-Ray bench lamp, 365 nm, 40 W) for 20 min. The solutions carrying microparticles used for low-cost microscopy imaging (Figure 2b), were not irradiated with a UV lamp, but with a 405 nm diode laser (200 mW, spot size 0.03 cm²) for 20 min. Then the particles were washed with water four times, allowed to sediment freely for 5 min between the washings.

Labeling Pharmaceutical Products: Tramadili hydrochloridum intravascular solution (Zentiva) was used as a model liquid pharmaceutical product. Approximately 50 particles dispersed in phosphate buffered saline (PBS) (50 µL) were pipetted into the solution. For a demonstration of the low-cost imaging, 50 particles of double size dispersed in PBS (50 µL) were pipetted into the solution and visualized using Neewer 60×–100× Optical Zoom Mobile Phone LED microscope. Stimorol Fusion Sugarfree gum was used as an OSD model. A droplet (≈20 µL) of water dispersion containing particles was placed on the surface of the OSD and was dried by using a nitrogen stream. Particles were visualized on the surface using a wide-field fluorescence microscope (Nikon Ti-E, Hg Intensilight source) set to RITC channel.

pH Sensing: Particles were dispersed in 0.1 M phosphate buffer of a pH 7.6 and the particle images were acquired with a fluorescence microscope (Nikon Ti-E, Hg Intensilight source) on FITC and RITC channel. The buffer was replaced with phosphate buffer of pH, 7.0, 6.5, 6.0, and 7.6, respectively. The interval between consecutive buffer replacements was 2 min, the microscope image was acquired every minute. The emission intensities were calculated from images (see image analysis section). The emission intensity of fluorescein was divided by the emission in intensity of rhodamine B, to give a ratiometric value.

Estimation of a Fluorescent Dye Content in a Labeled Product: No more than 100 microbarcodes were needed to label 1 mL of solution, the mass of one barcode particle is CA 75 pg (estimated from dimensions, density estimate ≈1.1 g mL^{-1}), which yields mass/mass concentrations for barcodes in the range of several ppm. The dye concentration is 100×10^{-6} M in the hydrogel (this is the concentration in the pregel, after polymerization, and washing, it will further drop), which corresponds to roughly 50 µg of the dye per 1 g of the hydrogel. It all together yields dye concentrations several orders of magnitude below 1 ppb (mass/mass) inside a solution labeled with these microbarcodes). In the case of pharmaceutical industry an undefined impurity in the formulation is tolerated as long as it does not exceed a daily dose of 1.5 µm g^{-1}. Expected amounts of the dye molecules were several orders of magnitude below this limit.

Particle Hydrolysis Experiments: Particles were stored at a given temperature in a PBS buffer with addition of 0.02% NaN$_3$ to inhibit bacterial growth and inspected periodically under the microscope in transmission mode using fluorescence microscopy (Nikon Ti-E, Hg Intensilight source) set to RITC channel.

Image Analysis: The fluorescence intensity of a particle was determined by averaging the intensity along a line perpendicular to the main axis of the particle using ImageJ software. Background intensity was subtracted. The intensities were averaged over five particles.

Supporting Information

Acknowledgements

Conflict of Interest

The authors declare no conflict of interest.

[1] WHO | Substandard, spurious, falsely labelled, falsified and counterfeit (SSFFC) medical products, http://www.who.int/mediacentre/factsheets/fs275/en/(accessed: July 2016).

[2] T. Kelesidis, I. Kelesidis, P. I. Rafailidis, M. E. Falagas, *J. Antimicrob. Chemother.* **2007**, *60*, 214.

[3] Background Information - FIP - International Pharmaceutical Federation Counterfeit medicines, http://www.fip.org/www/index.php?page=menu_counterfeitmedicines_policy (accessed: December 2016).

[4] Poisoned medicine kills dozens of children in Nigeria - CNN.com, http://edition.cnn.com/2008/WORLD/africa/12/18/nigeria.poison.drugs/(accessed: September 2016).

[5] Ensuring the Safety and Integrity of the World's Drug, Vaccine, and Medicines Supply, http://www.cfr.org/pharmaceuticals-and-vaccines/ensuring-safety-integrity-worlds-drug-vaccine-medicines-supply/p28256 (accessed: September 2016).

[6] V. N. Reports on Black market malaria medication could cause dramatic rise in disease's spread, http://vaccinenewsdaily.com/stories/510532765-black-market-malaria-medication-could-cause-dramatic-rise-in-disease-s-spread (accessed: September 2016).

[7] Y. Cheng, Y. Dong, J. Wu, X. Yang, H. Bai, H. Zheng, D. Ren, Y. Zou, M. Li, *J. Food Compos. Anal.* **2010**, *23*, 199.

[8] J. M. in Beijing, *Times Lond.* **2008**.

[9] Ministry: 6 infants possibly died of tainted milk powder_English_Xinhua, http://news.xinhuanet.com/english/2008-12/01/content_10441344.html (accessed: September 2016).

[10] WHO | IMPACT - The handbook, http://apps.who.int/impact/resources/handobook/en/index.html (accessed: September 2016).

[11] L. A. Felton, P. P. Shah, Z. Sharp, V. Atudorei, G. S. Timmins, *Drug Dev. Ind. Pharm.* **2011**, *37*, 88.

[12] D. Bansal, S. Malla, K. Gudala, P. Tiwari, *Sci. Pharm.* **2013**, *81*, 1.

[13] Edible Barcodes for Food Safety & Traceability Safe Traces, http://www.safetraces.com/(accessed: September 2016).

[14] M. Puddu, D. Paunescu, W. J. Stark, R. N. Grass, *ACS Nano* **2014**, *8*, 2677.

[15] S. O. Meade, M. S. Yoon, K. H. Ahn, M. J. Sailor, *Adv. Mater.* **2004**, *16*, 1811.

[16] DNA Based Bar Code for Improved Food Traceability, www.google.com/patents/WO2016114808A1?cl=en (accessed September 2016).

[17] TruTag Technologies - Product Authentication & Brand Protection, http://www.trutags.com/(accessed: September 2016).

[18] Taaneh: Authentication Technology, Anti Counterfeiting, Brand Protection Solutions, http://taaneh.com/(accessed: September 2016).

[19] J. S. Cybulski, J. Clements, M. Prakash, *PLoS One* **2014**, *9*, e98781.

[20] C. Huang, B. Lucas, C. Vervaet, K. Braeckmans, S. Van Calenbergh, I. Karalic, M. Vandewoestyne, D. Deforce, J. Demeester, S. C. De Smedt, *Adv. Mater.* **2010**, *22*, 2657.

[21] K. Braeckmans, S. C. De Smedt, C. Roelant, M. Leblans, R. Pauwels, J. Demeester, *Nat. Mater.* **2003**, *2*, 169.

[22] S. Han, H. J. Bae, J. Kim, S. Shin, S.-E. Choi, S. H. Lee, S. Kwon, W. Park, *Adv. Mater.* **2012**, *24*, 5924.

[23] D. Dendukuri, D. C. Pregibon, J. Collins, T. A. Hatton, P. S. Doyle, *Nat. Mater.* **2006**, *5*, 365.

[24] H. J. Bae, S. Bae, C. Park, S. Han, J. Kim, L. N. Kim, K. Kim, S.-H. Song, W. Park, S. Kwon, *Adv. Mater.* **2015**, *27*, 2083.

[25] Y. Zhao, Y. Cheng, L. Shang, J. Wang, Z. Xie, Z. Gu, *Small* **2015**, *11*, 151.

[26] a) D. C. Pregibon, M. Toner, P. S. Doyle, *Science* **2007**, *315*, 1393; b) Commericially available PEG barcodes from the company Fireflybio; http://www.fireflybio.com/(accessed: May 2017).

[27] Y. Zhao, H. C. Shum, H. Chen, L. L. A. Adams, Z. Gu, D. A. Weitz, *J. Am. Chem. Soc.* **2011**, *133*, 8790.

[28] H. Lee, J. Kim, H. Kim, J. Kim, S. Kwon, *Nat. Mater.* **2010**, *9*, 745.

[29] J. Lee, P. W. Bisso, R. L. Srinivas, J. J. Kim, A. J. Swiston, P. S. Doyle, *Nat. Mater.* **2014**, *13*, 524.

[30] Y. Zhao, Z. Xie, H. Gu, L. Jin, X. Zhao, B. Wang, Z. Gu, *NPG Asia Mater.* **2012**, *4*, e25.

[31] D. deKeiffer, *Am. J. Law Med.* **2006**, *32*, 325.

[32] M. You, J. Zhong, Y. Hong, Z. Duan, M. Lin, F. Xu, *Nanoscale* **2015**, *7*, 4423.

[33] M. You, M. Lin, S. Wang, X. Wang, G. Zhang, Y. Hong, Y. Dong, G. Jin, F. Xu, *Nanoscale* **2016**, *8*, 10096.

[34] E. Kang, G. S. Jeong, Y. Y. Choi, K. H. Lee, A. Khademhosseini, S.-H. Lee, *Nat. Mater.* **2011**, *10*, 877.

[35] Estimates of Foodborne Illness in the United States | Estimates of Foodborne Illness | CDC, https://www.cdc.gov/foodborneburden/(accessed: September 2016).

[36] World Health Organization, Foodborne Disease Burden Epidemiology Reference Group, *WHO Estimates of the Global Burden of Foodborne Diseases* **2015**.

[37] G. W. Frimpter, A. E. Timpanelli, W. J. Eisenmenger, H. S. Stein, L. I. Ehrlich, *J. Am. Med. Assoc.* **1963**, *184*, 111.

[38] M. S. Thakur, K. V. Ragavan, *J. Food Sci. Technol.* **2012**, *50*, 625.

[39] M. Smolander, E. Hurme, R. Ahvenainen, *Trends Food Sci. Technol.* **1997**, *8*, 101.

[40] X. Wang, H. Chen, Y. Zhao, X. Chen, X. Wang, X. Chen, *Trends Anal. Chem.* **2010**, *29*, 319.

[41] M. E. Helgeson, S. C. Chapin, P. S. Doyle, *Curr. Opin. Colloid Interface Sci.* **2011**, *16*, 106.

[42] D. Dendukuri, S. S. Gu, D. C. Pregibon, T. A. Hatton, P. S. Doyle, *Lab Chip* **2007**, *7*, 818.

[43] D. K. Hwang, J. Oakey, M. Toner, J. A. Arthur, K. S. Anseth, S. Lee, A. Zeiger, K. J. Van Vliet, P. S. Doyle, *J. Am. Chem. Soc.* **2009**, *131*, 4499.

[44] W. N. E. van Dijk-Wolthuls, S. K. Y. Tsang, J. J. Kettenes-van den Bosch, W. E. Hennink, *Polymer* **1997**, *38*, 6235.

[45] W. N. E. van Dijk-Wolthuis, J. A. M. Hoogeboom, M. J. Van Steenbergen, S. K. Y. Tsang, W. E. Hennink, *Macromolecules* **1997**, *30*, 4639.

[46] K. D. F. Vlugt-Wensink, R. de Vrueh, M. G. Gresnigt, C. M. Hoogerbrugge, S. C. van Buul-Offers, L. G. J. de Leede, L. G. W. Sterkman, D. J. A. Crommelin, W. E. Hennink, R. Verrijk, *Pharm. Res.* **2007**, *24*, 2239.

[47] J. A. Cadée, L. A. Brouwer, W. den Otter, W. E. Hennink, M. J. A. van Luyn, *J. Biomed. Mater. Res.* **2001**, *56*, 600.

[48] B. Orellana, A. M. Rufs, M. V. Encinas, C. M. Previtali, S. Bertolotti, *Macromolecules* **1999**, *32*, 6570.

[49] M. V. Encinas, A. M. Rufs, S. Bertolotti, C. M. Previtali, *Macromolecules* **2001**, *34*, 2845.

[50] S.-H. Kim, C.-C. Chu, *J. Biomed. Mater. Res., Part B* **2009**, *91B*, 390.

[51] L.-T. Ng, S. Swami, C. Gordon-Thomson, *Radiat. Phys. Chem.* **2006**, *75*, 604.

[52] S. Kim, C.-C. Chu, *Fibers Polym.* **2009**, *10*, 14.

[53] X. Wang, R. J. Meier, O. S. Wolfbeis, *Angew. Chem.* **2013**, *125*, 424.

[54] M. H. Lee, J. S. Kim, J. L. Sessler, *Chem. Soc. Rev.* **2015**, *44*, 4185.

[55] S. Schreml, R. J. Meier, O. S. Wolfbeis, M. Landthaler, R.-M. Szeimies, P. Babilas, *Proc. Natl. Acad. Sci. USA* **2011**, *108*, 2432.

[56] S. Bassnett, L. Reinisch, D. C. Beebe, *Am. J. Physiol.: Cell Physiol.* **1990**, *258*, C171.

[57] K. E. Sapsford, L. Berti, I. L. Medintz, *Angew. Chem. Int. Ed.* **2006**, *45*, 4562.

[58] D. J. Snodin, *Org. Process Res. Dev.* **2010**, *14*, 960.

[59] Temperature Monitoring & Temperature Sensitive Labels, http://timestrip.com/temperature-monitoring/(accessed: 2014).

[60] H. Z. An, E. R. Safai, H. Burak Eral, P. S. Doyle, *Lab Chip* **2013**, *13*, 4765.

[61] H. An, H. B. Eral, L. Chen, M. B. Chen, P. Doyle, *Soft Matter* **2014**, *10*, 7595.

[62] D. C. Appleyard, S. C. Chapin, R. L. Srinivas, P. S. Doyle, *Nat. Protoc.* **2011**, *6*, 1761.